Control and operation of a ship AC/DC microgrid under transient propulsion and manoeuvring load conditions

Hardan, Faysal; Norman, Rosemary; Tricoli, Pietro

DOI:
10.1016/j.ijepes.2021.107823

Document Version
Peer reviewed version

Citation for published version (Harvard):
Hardan, F, Norman, R & Tricoli, P 2022, 'Control and operation of a ship AC/DC microgrid under transient propulsion and manoeuvring load conditions', *International Journal of Electrical Power and Energy Systems*, vol. 139, 107823. https://doi.org/10.1016/j.ijepes.2021.107823

Control and operation of a ship AC/DC microgrid under transient propulsion and manoeuvring load conditions

Faysal Hardan[(1)*], Rosemary Norman[(2)], Pietro Tricoli[(1)]

[(1)] School of Engineering, The University of Birmingham,
Birmingham, B15 2TT, UK.
[(2)] School of Engineering, Newcastle University,
Newcastle upon Tyne, NE1 7RU, UK.
[*] Email: f.hardan@bham.ac.uk

Abstract

Moving towards more electric ships with sustainable designs can help in reducing the carbon footprint of the global transportation systems. Ship networks can be based on AC/DC microgrids with resilient structures to accommodate different types of power-generation and energy storage systems for supporting the dynamic loads of the vessel's propulsion and bow-thruster units. This paper presents a shipboard AC/DC microgrid with a super-capacitor (SC) system to support the ship's power system and to enhance its operational reliability under severe/transient loading scenarios, mainly arising from abrupt changes in the propulsion and bow-thruster power. A control system with SC voltage re-balancing mechanism is proposed for stabilizing the DC-bus voltage via bi-directionally power-controlled DC-DC converters utilizing the non-linear hyperbolic functions. The mechanism concurrently generates steady, slow-changing diesel-driven power through the microgrid voltage source converters to re-balance the SC voltage. The power system, including the diesel-generators, the microgrid components and the propulsion/thruster units, has been simulated in detail using the physical modelling-tools in the Matlab-Simulink® software, and run under harsh loading scenarios. The results demonstrated the effectiveness of the proposed control system with the microgrid structure and compared favourably with those obtained using other methods reported in the literature.

Keywords: AC/DC microgrid; ship power system; super-capacitor energy storage; VSC; propulsion

Nomenclature

BESS	Battery Energy Storage System
DES	Diesel Engine Generator
ESR	Equivalent Series Resistor
LV	Low Voltage
MV	Medium Voltage
MVDC	Medium Voltage Direct Current
PE	Power Electronic
RoCoT	Rate-of-Change of Torque
SC	Super-Capacitor
SCESS	SC Energy Storage System
VSC	Voltage Source Converter
VSI	Voltage Source Inverter
B	Mechanical damping factor [N.m/s]
C	Transfer function of the VSC and SC DC-DC converter

C_{dc}	DC-link capacitance [F]
C_{pid}	Transfer function of the SC voltage controller
C_{psc}	Transfer function of the SC current controller
C_{scc}	Transfer function of the SC DC-DC converter
C_{sc}	SC capacitance [F]
C_{vsc}	Transfer function of the VSC
DP_{ac}	DEG acceleration power [W]
DP_{dc}	Difference between the SC power and the DC load power [W]
F_{dc}	Transfer function of the DC-link capacitor
$F_{PLdc2Pvsc}$	Transfer function from DC-load power to VSC power
$F_{PLdc2Vdc}$	Transfer function from DC-load power to DC voltage
$F_{PLdc2Psc}$	Transfer function from DC-load power to SC power
$F_{PLdc2Vsc}$	Transfer function from DC-load power to SC voltage
$F_{PLdc2\omega m}$	Transfer function from DC-load power to DEG speed
$F_{Pvsc2\omega m}$	Transfer function from VSC power to DEG speed
F_{sc}	Transfer function of the SC
G_{dc}	DC-link conductance [1/Ω]
H_{dc}	DC-bus inertia constant [s]
H_g	DEG inertia constant [s]
i_{sc}^*	SC current reference
J	DEGs moment of inertia [kg.m^2]
k	Non-linear function parameter
K_{dr}	DC voltage droop-gain
K_{dv}	Differential gain of the SC voltage controller
K_i	Integral gain of the SC current controller
K_{iv}	Integral gain of the SC voltage controller
K_p	Proportional gain of the SC current controller
K_{pv}	Proportional gain of the SC voltage controller
K_{vsc}	Per-unit conversion factor
P	VSC AC power [W]
P_{Ldc}	DC load power [W]
P_{sc}	SC power [W]
P_{sc}^*	SC power reference or demand
P_{vsc}	VSC DC power [W]
S_{gn}	Generators' nominal VA power [VA]
S_{vscn}	VSC nominal VA power [VA]
V_{dc}	DC-bus voltage [V]
V_{dcn}	DC-bus nominal voltage [V]
V_{sc}	SC voltage [V]
V_{sc}^*	SC voltage reference
ρ_{vsc}	VSC conversion efficiency
τ	Time constant [s]
ω_m	DEG speed [rad/s]
ω_{ms}	DEG synchronous speed [rad/s]

1. Introduction

Microgrids have long been considered for, and demonstrated in, projects around the world where they can include various types of distributed energy sources (DESs) such as renewable power units, energy storage systems, and rotating generators [1], [2]. They can be configured within local medium/low voltage (MV/LV) networks or power

systems, and can operate in both grid-connection and standalone modes to ensure security of power supply, in addition to other merits such as contributing to a reduction in carbon emissions [3]. Their optimised design and control, and coordinated operation of the power generators and sources connected to the network have been actively researched, pushing the boundaries to improve performance and reliability [4]-[8].

To accommodate various type of energy sources, these microgrids can be expanded with DC networks that interconnect with the AC networks through power electronic (PE) converters/inverters, mainly voltage source converters (VSC). The DC network also gives the microgrid greater flexibility in terms of accommodating battery energy storage systems (BESS) and multi-level DC capability using DC-DC converters [9]-[11]. Such microgrids are currently known as AC/DC microgrids, although DC microgrids have been separately studied and reported in the literature, e.g., in [12].

Being flexible and with the potential to be designed and configured for standalone and grid-connected applications, these AC/DC microgrids have been considered for application on ships with different hybrid architectures [13]-[17]. Review studies covering their characteristics, power electronic components, standard architectures, technical considerations and key advantages for utilisation in ships have been covered in the literature [14], [18]-[20]. The ship microgrid is inherently isolated when providing power to the vessel at sea, and it is mainly powered through its prime movers, typically diesel engine generators (DEG), which determine the working frequency of the AC supply on-board, and regulation of this frequency is achieved through controlling the speed of the rotating generators. Ship manoeuvrability requires a high dynamic response and, for vessels with electrical propulsion, the loads reflected on the generators can be high and of a pulsating nature, which can cause a significant drop in the generator speed unless an additional generator is brought online. If the load power is immediately consumed from the DC bus, a steep drop in the DC voltage below its standard limit may easily occur [18]. Therefore, optimal design, control and coordination of energy storage systems for maintaining the DC bus voltage of the ship microgrid are required [21]-[26]. In order to provide high dynamic response of the vessel, paper [21] presents an optimal design methodology for hybrid-electric power systems on board, which focused on economic objectives. Reference [22] proposed an intelligent coordination algorithm to mitigate the effect of pulsating loads on a 5kV MVDC bus that ensures an appropriate sharing of power amongst the energy storage units. Paper [23] considered a passive hybrid topology for a ship microgrid based on parallel connection of batteries and super-capacitors, demonstrating that the DEG delivers constant power whilst the energy storage units stabilize the DC-link voltage. In [24], an energy storage management system based on fuzzy-logic was proposed for supporting an MVDC shipboard power system, whilst in [25] the authors proposed a hybrid energy storage system of batteries and ultra-capacitors connected immediately to the bow-thruster drive and controlled respectively via low- and high-pass filters inside a primary controller. To meet the control and management requirements for a shipboard power system with a DC distribution network, reference [26] proposed a hierarchical control design, in which a frequency-division method (similar to the method of [25] - low/high-pass filters) was used for enabling the operation of the hybrid energy storage system. Controlling and managing issues for such systems based on batteries and super-capacitors, including their optimization, control and structures in general, are reviewed in reference [27].

The contribution of this paper covers several aspects of ship AC/DC microgrids, with the main focus being on the utilization of short-term energy storage systems, represented by super-capacitor (SC) technology, and their power-electronic converters for stable and reliable operation of the microgrid under harsh dynamic loading. These include a new method for controlling and stabilizing both the DC-bus voltage and AC-bus frequency, in addition to new dynamic-system analysis and design, which contribute to filling research gaps in the area and to enhancing the control performance of the vessel's power and propulsion systems. In comparison with batteries, SCs are an attractive solution as they can provide very-high transient currents with low equivalent series resistance (ESR) giving higher system efficiency, and they have long operational lifetimes with typically a million charging/discharging cycles [28]. A microgrid architecture including the DEGs and the SC energy storage system (SCESS) with 20F capacitance has been developed to achieve optimized dynamic operation in terms of worst-case DC-loading scenario. A fast controller for stabilising the DC-bus voltage through exchanging the DC power with the SC has been proposed and designed utilizing nonlinear functions of a suitable order. A slow outer control-loop for re-balancing the SC voltage is also proposed to address the gradual increase/decrease in the DEG load when the DC load is high and pulsating. As a result, variations in the DEG frequency/speed and in the DC-bus voltage are kept within the standard limits, [29], and the frequency of the AC grid was found to be far from reaching these limits under all presented testing conditions. These test results were compared with those obtained when using the high-pass filter method for producing the power reference of the SC, as documented in references [25], [26]. It was demonstrated that the proposed control method, within the considered microgrid structure, provided improved performance and characteristics when compared with those reported in these references, as discussed quantitatively in section 8. The methods in [25] and [26], and a similar technique in [30] which also utilized a high-pass filter for producing power demand to a flywheel energy storage system, were all implemented in an open-loop manner and they cannot prevent the SC voltage or the flywheel speed from shifting down or biasing. In comparison, the proposed method is based on closed-loop control that guarantees the re-balancing of the SC voltage and prevents the voltage from drifting down whilst the system is running.

The paper is organized in the following manner. Section 2 presents and explains the proposed structure of the ship AC/DC microgrid including the prime movers and the propulsion and bow-thruster units. Section 3 discusses the modular representation of the ship power system and its components whilst section 4 models and analyses the mutual effects between the AC and DC grids. In section 5, the purpose and characteristics of the nonlinear functions are discussed, and in section 6, the control structure of the SC DC-DC converter is discussed in detail. Frequency and time-domain analysis of the DC-bus voltage control system are presented in section 7. System simulation, results and their analysis with comparison to the literature are presented in section 8. Finally, conclusions are drawn in section 9 with some remarks.

2. The architecture of the ship power system

In this paper, the system architecture including the ship powertrain illustrated by the single-line diagram in Fig.1 was used, which integrates the SCESS into the DC-bus to support the DC voltage and AC-bus frequency as part of the ship's AC/DC microgrid. This architecture was designed to fulfil all power requirements for the ship's electric

propulsion system, its bow-thrusters and service load. Both thrusters are rated at 0.25MVA each utilizing a voltage source inverter (VSI) based field-oriented or vector-controlled induction-machine drive for high-response torque performance, [31], which is a requirement for ship manoeuvrability. The propulsion system consists of twin-screw propellers, each driven by a 1000HP (0.75MVA) induction-machine drive that also operates with high-performance using the vector-control technique. These drives, for both the thrusters and the propellers, are powered through the DC-bus and their loads sum up to a 2MW maximum power at any operational instant. Accordingly, the SCESS was

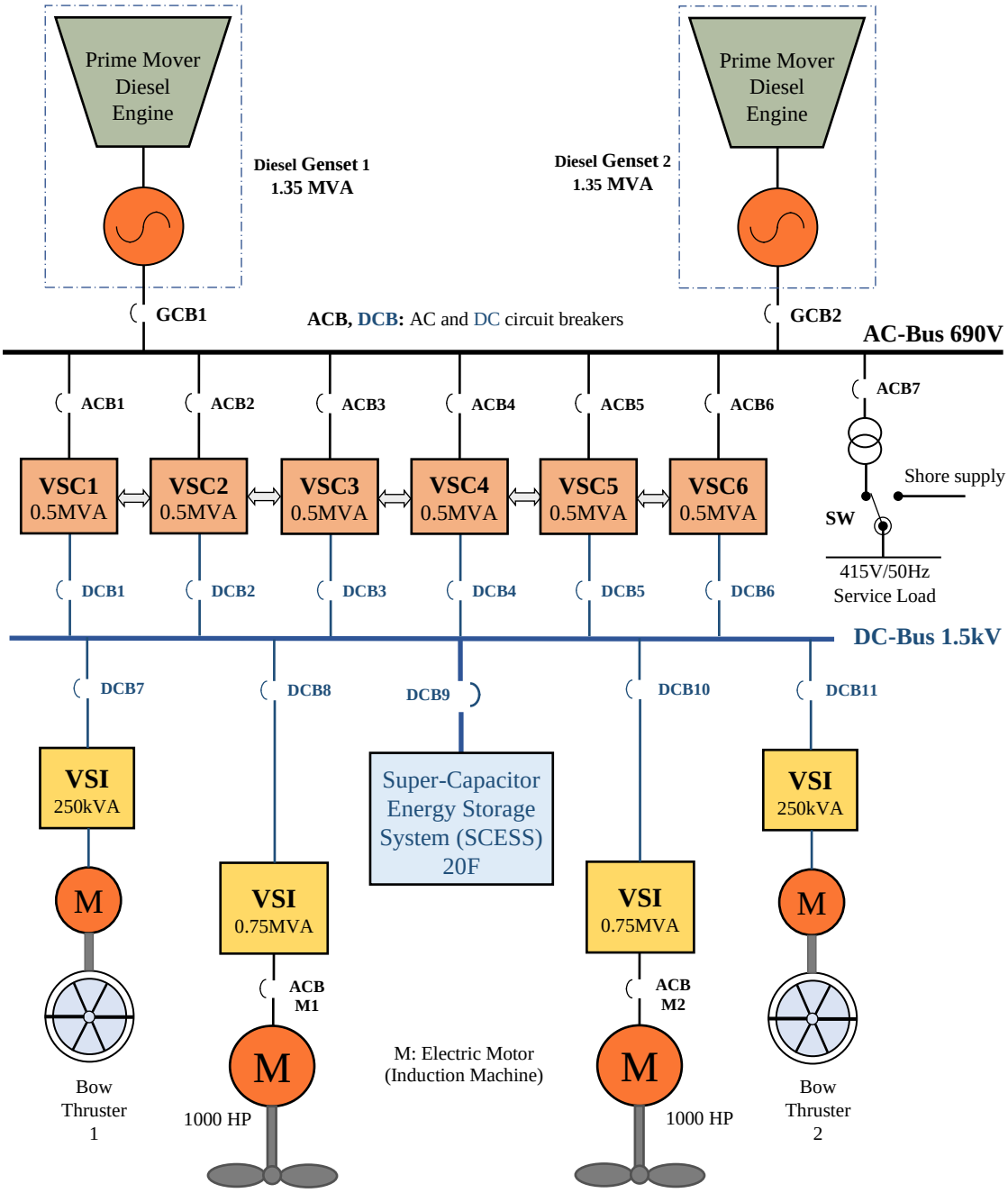

Fig. 1. A single-line block diagram of the vessel's AC/DC power system including powertrains considered for the paper's case study

rated at 3MW with 50% power margin capability as it relies on PE converters, and to securely tolerate the maximum transient power of the propellers and thrusters. The DEGs were rated at 1.35MVA each which can also cover the AC service load of the ship. To allow for connection of a cold ironing or shore supply when the ship is in port, a two position AC switch (SW) is provided to connect the ship's service load to an onshore electrical network.

In order to power the DC-bus, six 0.5MVA VSCs were utilized to form bridges between the AC and DC buses and to share the total AC/DC current between them with the capability of bidirectional power flow. Each VSC operates at a switching frequency of 2,250Hz and all switching waveforms for the VSCs are interleaved to produce smooth fundamental current waveforms, which considerably reduces the VA rating of the harmonic filter used on the AC side. To interleave the VSCs, their switching-frequency waveforms are shifted by $2\pi/6$ rad with respect to each other. The voltage ratings of the AC-bus and DC-bus were set at 690V and 1.5kV, respectively, to allow power distribution with lower currents and to comply with the standards for ship electrical power systems [29]. The SCESS is equipped with a bidirectional power-controlled DC-DC converter (buck-boost type, [32], [33]) in order to control the power flow into and out of the SC module. The technical specifications of the SCESS are given in Appendix A.

3. System modular units and operation concept

The ship's power system considered in this study, as shown in Fig. 1, can be represented by a simplified block diagram with three main units as shown in Fig. 2. These units are: the SC and its bidirectional DC-DC converter, the DC load that represents the propulsion and bow-thruster loads, the DC-link capacitor and the VSC including its high-pass harmonic filter. The DC-DC converter is composed of the six interleaved 0.5MW DC-DC converters connected in parallel, which share the total current amongst them. Both the DC-DC converter and the VSC have their own power controllers designed with typical response times in the range from 1.5ms to 3ms. For the VSC, power control is possible using different techniques, [34]-[38], but the method in [34] was adopted for this paper due to its modular design using a simple per-unit structure. Details of the power controller for the DC-DC SC converter are presented in section 6.

Using the notations for power flows and directions for each unit as illustrated within the block diagram in Fig. 2, it can be realised that in order to regulate the DC-bus voltage, the power flow into the DC-link capacitor must be controlled as tightly as possible in response to any uncertain and sudden changes in the DC load. The control action must also guarantee that the DC voltage does not drift beyond the standard limits of ±10%. Accordingly, the proposed control method was set to take advantage of the DC voltage tolerance ±10% limits by allowing the SC DC-DC converter to control the power flow (P_{sc}) into and out of the DC-link capacitor, whilst letting the diesel generators gradually ramp up their power (P) to supply the DC-bus. This mechanism in turn prevents the speed or frequency of the DEGs from dropping below the recommended limit of 5% for ship power systems [18]. In rare circumstances, and for protection, if the SC state-of-charge is low and its voltage reaches the lower limit, the SCESS must be able to issue a signal to limit the rate-of-change of torque (RoCoT) demands for the propulsion or thruster drives (i.e., the DC load) and allow the DC-link voltage to build up by accumulating more power from the DEGs (P_{vsc}). To control the SC power flow, linear and non-linear functions were utilized to generate power references for the SC DC-DC converter, whilst the VSC power demand was made available as an output of a non-linear PI controller

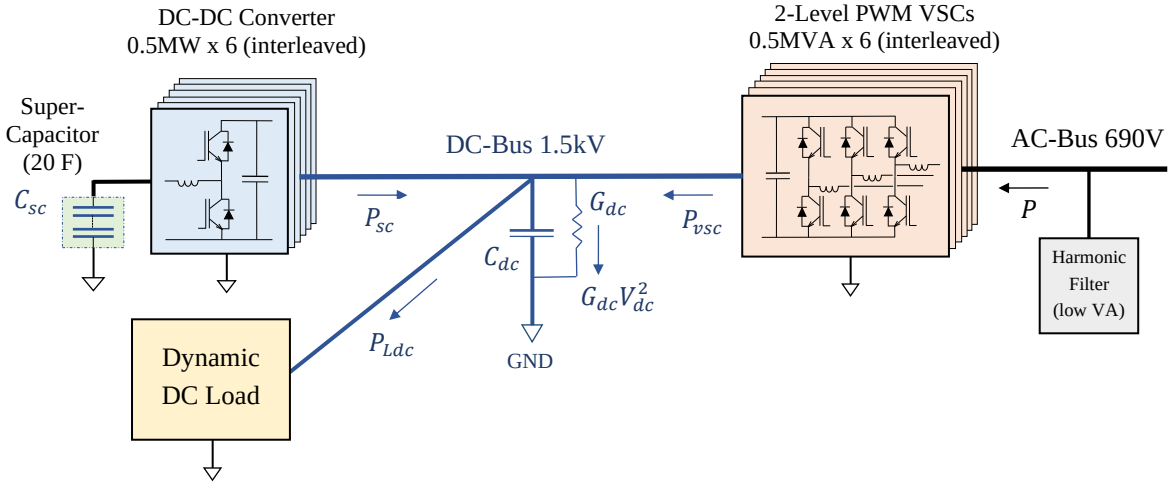

Fig. 2. A representation of the DC-bus circuit and its connected components

applied to control or re-balance the SC voltage. Such a controller must be designed and tuned to provide a slow changing/ramping output (as P_{vsc}^{*}) in one direction, causing P_{vsc} to flow towards the DC-link capacitor whilst re-balancing the SC voltage within a minimum time sufficient for the DEGs to produce the required mechanical power without causing their speed to drop below the lower limit.

4. Mutual effect between AC and DC grids

To quantify the mutual effect between the DC- and AC-buses of the ship power system, an electromechanical model that combines the DC voltage and the DEG speed was firstly derived as follows. The per-unit power-speed model of the total rotating generation capacity can be described around the synchronous speed ω_{ms} as [39],

$$\frac{d\omega_m}{dt} = \frac{1}{2\,H_g}\,(DP_{ac} - P) - \frac{B}{J}\omega_m\,, \qquad (1)$$

where, DP_{ac} is the difference between the generators' mechanical power P_m and the AC load power P_{Lac}, P is the power supplied to the VSC, ω_m, B are the generators' speed and mechanical damping-factor, and H_g is the inertia constant of all rotating generators which is defined as,

$$H_g = \frac{\frac{1}{2}J\,\omega_{ms}^2}{S_{gn}}; \quad (2)$$

J, ω_{ms} and S_{gn} are the generators' total moment of inertia, nominal speed and VA power, respectively.

Aiming for a similar form to the power-speed dynamic model of the generator as given in (1), the following per-unit power-voltage model of the DC-bus source can also be derived,

$$\frac{dV_{dc}}{dt} = \frac{1}{2\,H_{dc}}\,(DP_{dc} + P_{vsc}) - \frac{G_{dc}}{C_{dc}}V_{dc}\,, \quad (3)$$

where, DP_{dc} is the difference between the SC power P_{sc} and the DC load power P_{Ldc} (i.e. $DP_{dc} = P_{sc} - P_{Ldc}$), P_{vsc} and G_{dc} are respectively the power supplied to the DC capacitor by the VSC and the DC-bus parallel conductance, and H_{dc} is the inertia constant of the DC-bus which can be defined as,

$$H_{dc} = \frac{\frac{1}{2} C_{dc} V_{dcn}^2}{S_{vscn}}; \qquad (4)$$

C_{dc}, V_{dcn} and S_{vscn} are the DC-bus total capacitance, its nominal voltage and the nominal VA power of the VSC, respectively. In (1) the AC power P supplied to the VSC can be written as $P = K_{vsc}\, P_{vsc}$ according to Fig. 2, where K_{vsc} is the per-unit transfer factor between the DEGs' power and the VSC power and can be calculated as,

$$K_{vsc} = \frac{VSC\ nominal\ power}{DEG\ nominal\ power} = \frac{3\times10^6}{2.7\times10^6}.$$

The power-conversion efficiency of the VSC is assumed to be very-high and equal to one for calculation purposes. As the VSC is designed with power-control capability, its power, P_{vsc} can be considered as an input control variable whereas DP_{ac} and DP_{dc} can be assumed constant or to act as system disturbances for the analysis. Therefore, by linearizing around the nominal generator speed and DC-bus voltage, Eq. (1) and Eq. (3) become,

$$\frac{d\Delta\omega_m}{dt} \cong \frac{-K_{vsc}\,\Delta P_{vsc}}{2\,H_g} - \frac{B}{J}\Delta\omega_m\,; \qquad (5)$$

$$\frac{d\Delta V_{dc}}{dt} \cong \frac{\Delta P_{vsc}}{2\,H_{dc}} - \frac{G_{dc}}{C_{dc}}\Delta V_{dc}\,; \qquad (6)$$

For transient analysis within the first second following a loading event, the change in the DEG mechanical power can be ignored for (5) due to the slow response of the DEG and, therefore, it has no effect on the generator speed within this time interval. Combining (5) and (6) by eliminating ΔP_{vsc} in both equations, and converting the resulting relationship between the generator speed and the DC-bus voltage to the s-domain, it can be found that,

$$\Delta\omega_m(s) \cong \frac{-K_{vsc}\,H_{dc}}{H_g}\,\frac{(s+\frac{G_{dc}}{C_{dc}})}{(s+\frac{B}{J})}\Delta V_{dc}(s), \qquad (7)$$

$$\Delta V_{dc}(s) \cong \frac{-H_g}{K_{vsc}\,H_{dc}}\,\frac{(s+\frac{B}{J})}{(s+\frac{G_{dc}}{C_{dc}})}\Delta\omega_m(s). \qquad (8)$$

It can be realised that (7) and (8) possess the characteristics of phase lead-lag and lag-lead, respectively, and the response of the speed to a step change in the DC-bus voltage is ideally instantaneous, i.e. any drop in the DC-bus voltage as a result of DC-bus loading will be reflected immediately on the DEG speed, and vice-versa according to (8). This speed response to a 0.01pu step in the DC-bus voltage is equal to $-0.01\,K_{vsc}\,H_{dc}/H_g$ at the time instance when the step in the DC-bus voltage takes place, according to (7). Using the parameters as given in Appendix A for the system in Fig.1, this response will be equal to 0.00656pu. Therefore, delaying the change in DC-bus voltage utilizing the SC system with high-response DC-DC power controller will enable a smooth operation of the DEGs under all loading conditions, particularly under severe transient loading resulting from high and sudden torque demands applied to the propulsion and bow-thruster drives.

5. Non-linear functions for power control

It is usual to have a voltage-droop control for the DC-bus with a suitable gain according to the permitted DC voltage limits [29]. As the DC-voltage maximum tolerance is ±10%, the voltage-droop gain, K_{dr} must be higher than 10 in order to generate ±1pu power for the DC-link capacitor before the DC voltage shifts completely by ±0.1pu. This gain can be represented via the voltage droop line (line 1), as illustrated in Fig.3. Accordingly, the per-unit power reference for controlling the DC voltage via the SC DC-DC converter can be derived as,

$$P_{sc}^{*} = K_{dr}\,(V_{dc}^{*} - V_{dc}) = K_{dr}\,e = f_1(\mathrm{e}); \qquad (9)$$

where, e is the DC-voltage error.

It is considered that whilst P_{sc}^{*} regulates the DC-bus voltage, the VSC power P_{vsc} is constant or changing slowly in comparison with the dynamics of the DC-bus voltage. As the power demand P_{sc}^{*} in (9) is a linear function of the DC voltage error, higher order or non-linear odd functions can also be used to add different features to the control process of the DC voltage, e.g. as illustrated by curves 2 and 3 around line 1 in Fig. 3. As such, these functions will also be able to generate a bidirectional power demand P_{sc}^{*} with very low or high gains near zero voltage-error, but they will result in maximum values for P_{sc}^{*} when the voltage error is close to ±0.1pu. The curve functions can be represented by polynomials of odd orders such as those of 7th and 9th orders in terms of the DC voltage error. Suitable hyperbolic tangent functions and their inverse counterparts with some design parameters can also be possible, which were adopted in this study to demonstrate the concept. Details of the testing of a wide variety of relevant curve functions for the selection process are beyond the scope of this paper. Accordingly, in Fig. 3, f_2 was designed to embody a hyperbolic tangent function whilst f_3 was considered as the inverse function of f_2, and all associated dashed and dashed-doted curves are obtained at different function parameters, as explained below. As can be demonstrated via Fig.3, the curves are able to generate the power demand P_{sc}^{*}, and the selected functions can be represented by,

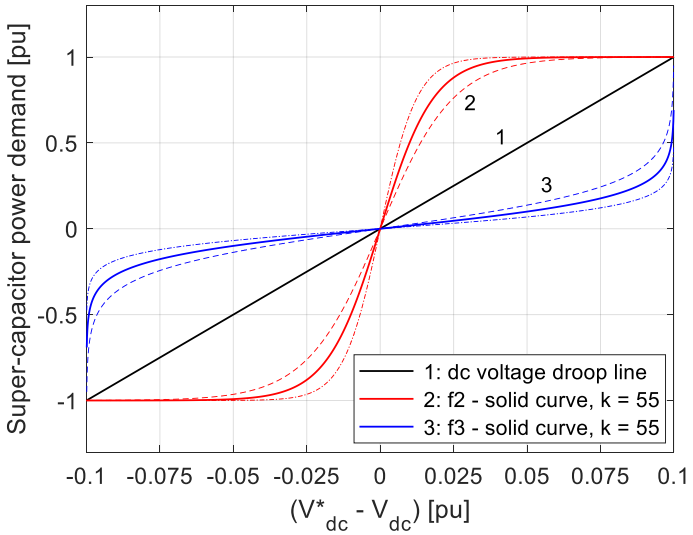

Fig. 3. The control functions that produce the power command for the super-capacitor DC-DC power converter

$P_{sc}^{*} = f_2(V_{dc}^{*} - V_{dc}) = f_2(e)$, or, (10)

$P_{sc}^{*} = f_3(e)$, (11)

It can be realised that function $f_3(e)$ generates a low power demand P_{sc}^{*} in the region close to the DC voltage reference V_{dc}^{*} which makes better utilisation of the DC-bus stored energy before reaching the DC voltage limits. In contrast, function $f_2(e)$ generates a higher P_{sc}^{*} within the same region, providing better DC voltage stabilization but does not exploit the DC-bus stored energy, which leads to an increase in the magnitude of P_{sc}^{*} for the DC-DC controller of the SC unit. Curves 2 and 3 can be described mathematically using the following forms which account for mapping the input range $\{-0.1 \cdots + 0.1\}$ of the DC voltage error to an output range $\{-1 \cdots + 1\}$ that represents the per-unit power demand, P_{sc}^{*}.

$f_2(e) = tanh\{k.(V_{dc}^{*} - V_{dc})\}$, or

$f_2(e) = \frac{1-e^{-2k\cdot(V_{dc}^{*}-V_{dc})}}{1+e^{-2k\cdot(V_{dc}^{*}-V_{dc})}}$, (12)

$f_3(e) = 10 \cdot atanh\{10.(V_{dc}^{*} - V_{dc})\}/k$, or

$f_3(e) = \frac{\left\{ln\left(1+(V_{dc}^{*}-V_{dc})\right)-ln\left(1-(V_{dc}^{*}-V_{dc})\right)\right\}}{2k}$, (13)

where, k is the functions' parameter. The curves shown in Fig. 3 are produced for $k = 55$ (solid lines), $k = 40$ (dashed lines) and $k = 80$ (dashed-dot lines).

It should be noted that for implementation purposes the designed curves for $f_2(e)$ and $f_3(e)$ can be embedded within look-up tables using a certain number of data points over the full input/output ranges with a suitable interpolation mechanism.

6. The control structure of the super-capacitor DC-DC converter

In order to prevent the SC voltage from exceeding its maximum and minimum limits and allow the SC unit to function properly in both power directions, hysteresis functions (HFs) were developed to adaptively set the current upper and lower limits of the SC according to its voltage level, as shown in Fig. 4. The hysteresis function of graph (a) is for setting/adapting the current upper limit I_{UL} as a function of V_{sc}, whilst the hysteresis function of graph (b) is similarly used but for the current lower limit I_{LL}. To implement these hysteresis functions, V_{sc} is used to derive the initial current demand i_{sci}^{*} from the power demand P_{sc}^{*}, as illustrated within the structure of the DC-DC converter's power-controller shown in Fig. 5. If the SC voltage exceeds its maximum limit, V_{max}, the hysteresis function $I_{UL}(V_{sc})$ will only permit a current demand in the positive direction, or a current that will only discharge the SC by restricting the final current demand within a range from 0 to MAX level. Similarly, but in the opposite direction, if the SC voltage drops to a level below its minimum limit, V_{min}, the hysteresis function $I_{LL}(V_{sc})$ will only permit a current demand in the negative direction, within a range from MIN to 0 level, to charge the SC. As shown, the hysteresis functions update the current limiter of the reference current i_{sc}^{*} that passes to a closed-loop current-control structure using the controller function $C_{psc}(s)$, which was selected as a PI type to produce the voltage-

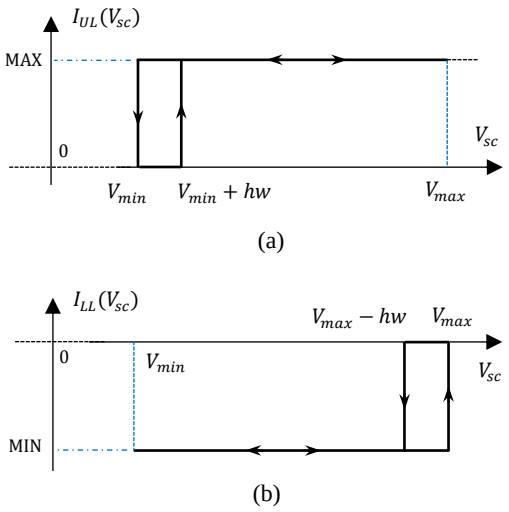

Fig. 4. the hysteresis functions (HFs) for setting /updating the upper and lower limits for the SC current according to the SC voltage level, (a): for the upper limit, (b): for the lower limit

difference reference ΔV^*_{pwm}. The latter is then added to the measured SC voltage in order to obtain the voltage reference V^*_{pwm} for the DC-DC converter. When the SC voltage hits one of its limits, or when one of the SC current limits becomes zero, the DC load must be restricted to change slowly in order to prevent the collapse of the DC-voltage, as the SC is no longer able to dynamically support DC-voltage stabilization under this condition. Although such a condition would only occur in rare events, a protective measure has been considered by issuing a signal through the HFs block, when one of the current limits is zero, to limit the RoCoT for the propulsion or thruster drives, as shown in Fig. 5. It should be noted that as the SC voltage is a very slow-changing variable with respect to the SC current, fixed parameters for the $C_{psc}(s)$ were derived around the voltage operating-point of the SC, based on the DC-DC converter model. By considering the per-unit values of the controller variables, and that a typical current/power step-response of around 2ms is sought, the controller $C_{psc}(s)$ was designed with fixed proportional and integral gains, respectively as $K_p = 0.01$ and $K_i = 10$.

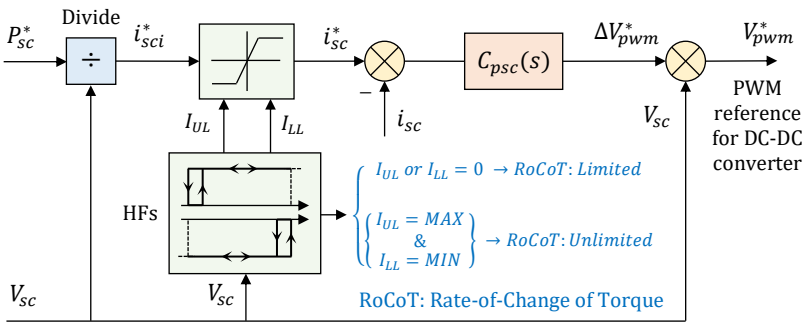

Fig. 5. Block diagram representing the super-capacitor power/ current controller including hysteresis functions and RoCoT signal

7. Analysis of the DC-bus-voltage control system

The close-loop control system including system models and controllers has been constructed and represented by the block-diagram as shown in Fig. 6. It was used to analyse and verify the characteristics and performance of the DC-bus voltage controller, utilizing the proposed super-capacitor control concept, and to select the most suitable value for the DC-link capacitor. It should be noted that the SC voltage controller $C_{pid}(s)$ must be selected with a memory component, such as an integrator, in order to sustain a controller output for demanding the VSC power that balances the total DC-load whilst leading to zero steady-state error in the SC voltage. Such features can be fulfilled using the proportional-integral-differential (PID) structure for the $C_{pid}(s)$ as adopted in this design study. The system block-diagram was also used to derive a perturbation model of the system around the nominal values of the DC-bus and SC voltages or their references. For a linear presentation, the voltage-droop gain K_{dr} (line 1 in Fig. 3) was considered for this analysis as demonstrated in Fig. 6. From the block-diagram, the following transfer functions in the s-domain can be derived,

$$F_{PLdc2Vdc} = \frac{\Delta V_{dc}}{\Delta P_{Ldc}} = \frac{-F_{dc}}{1 + K_{dr}\, C\, F_{dc}\, [1 - C_{pid}\, C\, F_{sc}]}, \quad (14)$$

$$F_{PLdc2Pvsc} = \frac{\Delta P_{vsc}}{\Delta P_{Ldc}} = \frac{-F_{dc}\, K_{dr}\, C_{pid}\, C^2\, F_{sc}}{1 + K_{dr}\, C\, F_{dc}\, [1 - C_{pid}\, C\, F_{sc}]}, \quad (15)$$

$$F_{PLdc2Vsc} = \frac{\Delta V_{sc}}{\Delta P_{Ldc}} = \frac{F_{dc}\, K_{dr}\, C\, F_{sc}}{1 + K_{dr}\, C\, F_{dc}\, [1 - C_{pid}\, C\, F_{sc}]}, \quad (16)$$

$$F_{PLdc2Psc} = \frac{\Delta P_{sc}}{\Delta P_{Ldc}} = \frac{F_{dc}\, K_{dr}\, C}{1 + K_{dr}\, C\, F_{dc}\, [1 - C_{pid}\, C\, F_{sc}]}, \quad (17)$$

where the notation '(s)' of all functions is dropped to simplify the presentation.

The derived functions were utilized to design and tune the parameters of the SC controller in addition to selecting the value of the DC-bus capacitor C_{dc}. The SC value, which is the main parameter of $F_{sc}(s)$, was determined based on the following design setting: the SC voltage should not be allowed to drop by more than 40% from its rated value (900V) during the first 5s after applying a DC current step corresponding to the maximum propulsion and thruster power (i.e. 2MW or 0.666pu). Accordingly, a value of 20F for the SC was found to be sufficient for satisfying the

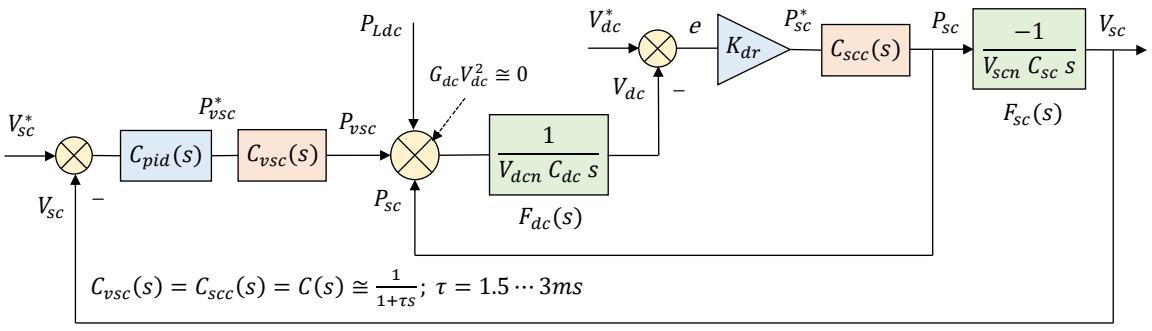

Fig. 6. A block-diagram representing the close-loop of the DC-bus and SC voltage controllers for modelling, analysis and design, using the proposed super-capacitor control concept

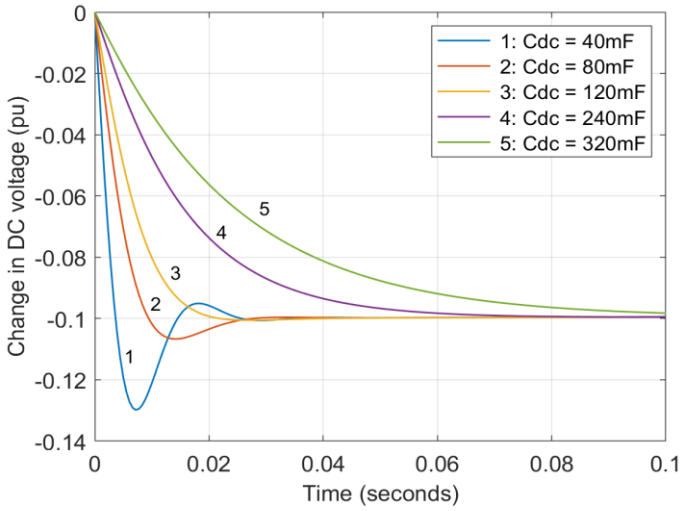

Fig. 7. The DC-bus voltage response to a maximum step in DC-bus load (1pu) for different values of the DC-link capacitor C_{dc}

above design requirement. To get an initial design value for the DC-bus capacitor C_{dc}, it was assumed that under a worst-case delay in the SC power response, which was assumed 3ms, the C_{dc} nominal voltage should not drop to a level below its lower limit (1350V) when a DC-load power-step equal to the rated power is supplied by DC-bus. Considering this condition, an initial value of 40mF was found for C_{dc} and used as an initial design value. For selecting the most suitable gains of the $C_{pid}(s)$, the frequency and time responses of the above functions were used. The selected gains are listed in Appendix A. Utilizing the function in (14), with the selected gains and relevant parameters given in Appendix A, the DC-bus voltage response to a full-load step in the DC-bus power, for different values of C_{dc}, was calculated and depicted in Fig.7. It can be realised that the larger the C_{dc} value used, the higher the performance can be obtained in terms of regulating the DC-voltage. Substituting the parameters and gains in Eqs. (15)–(17) for their selected values, the step-responses of the DC-bus voltage, VSC power, SC voltage and power, in addition to the generator speed/frequency, were all derived and presented in Fig. 8 under maximum step in the DC-load. It can be realized that these responses conform to the expected system performance, according to the design limits and parameters, within the presented time-range.

Based on Eq. (5), the perturbation power-speed model in the s-domain, around the synchronous speed and under constant DP_{ac}, can be derived as,

$$F_{Pvsc2\omega m} = \frac{\Delta\omega_m}{\Delta P_{vsc}} = \frac{-K_{vsc}}{2H_g\,\rho_{vsc}\,(s+\frac{B}{J})}; \qquad (18)$$

Multiplying Eq. (18) by Eq. (15) gives,

$$F_{PLdc2\omega m} = \frac{\Delta\omega_m}{\Delta P_{Ldc}} = \frac{-K_{vsc}}{2H_g\,\rho_{vsc}\,(s+\frac{B}{J})} \cdot \frac{-F_{dc}\,K_{dr}\,C_{pid}\,C^2\,F_{sc}}{\{1+K_{dr}\,C\,F_{dc}\,[1-C_{pid}\,C\,F_{sc}]\}}, \qquad (19)$$

which can represent the frequency-response of the generator speed to any change in the DC-load. Utilizing this function with the function of Eq. (15), the responses of the generator speed and VSC power can be depicted as shown

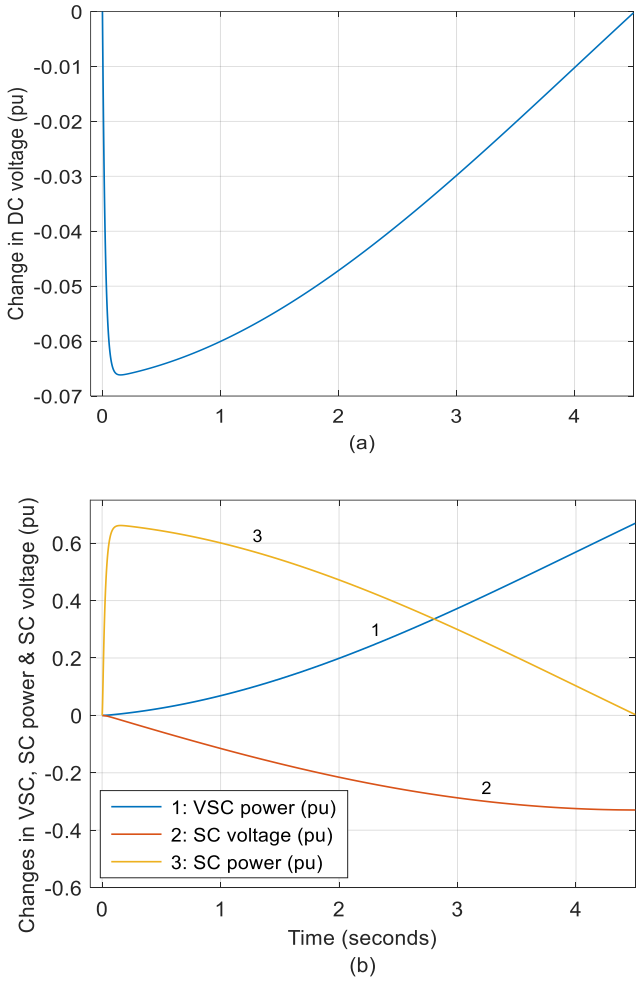

Fig. 8. (a): DC-bus voltage response to a maximum step in the propulsion DC-load (0.666 pu), (b): the VSC power and SC voltage & power responses to the same step in the DC-load.

in Fig. 9. It can be noticed that because the VSC power is forced to ramp up slowly as a response to the large step in the propulsion DC-load, there is a corresponding slow variation in the generator speed which is around 4% at a time of 1s. However, when the response of the generator-engine starts to build up to regulate the generator speed, the latter will recover towards its nominal value and the action of the SC re-balancer will gradually transfer the generator power via the VSC to the propulsion DC-load through the DC-bus.

8. System tests, results and analysis

Under harsh and transient DC loading conditions exerted by the propulsion and bow-thruster units, the DC-bus voltage can drop suddenly to a level below the permitted lower limit. This extreme condition could cause the whole AC/DC ship power-system to shut down as a result of activating the protective circuit breakers and devices unless a limit on the rate of change of the electrical load is introduced. Such a limit is usually adopted in typical ship systems, [40], [41], which adversely affects the dynamic performance of the ships and their manoeuvrability. However, as

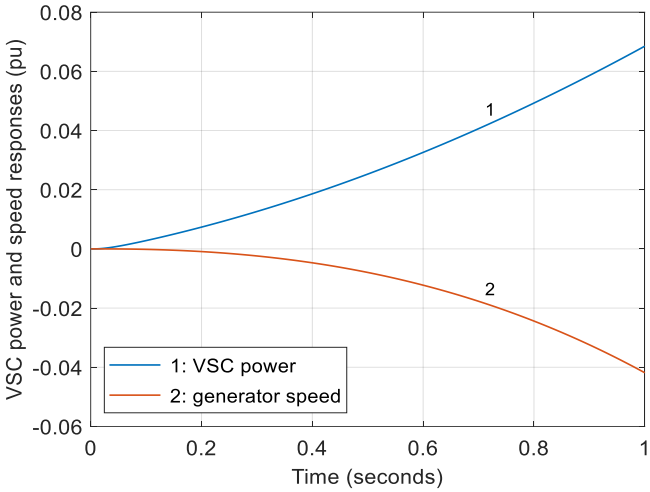

Fig. 9. The responses of the generator speed and VSC power to a maximum step in DC propulsion load for 1s when there is no change in power contribution from the diesel engine

the vector-controlled drives for the propulsion and bow-thruster units are designed to provide high-torque response (typically within few milliseconds), it would be highly recommended to test the proposed control system under extreme torque demands applied to these drives, without imposing any rate limit on the torque for high-dynamic positioning. For this, the whole ship power system and its components, including the propulsion and bow-thruster units, have been simulated utilizing the physical modelling and simulation tools of the Matlab-Simulink® software. The proposed controllers were then added and activated for testing under different torque or DC-loading scenarios to validate the control system operation and performance, and to compare its performance with those obtained using the other methods reported in the literature.

8.1. Testing and comparing the performance using the non-linear functions

To clearly demonstrate the difference in the system performance when using the non-linear functions f_1(e), f_2(e) and f_3(e), three simulated power systems, each implemented with one of the functions were run in parallel. The recorded results are shown in Fig. 10. As the differences in the SC power and the voltage fluctuation in the DC-bus can be more clearly seen at a lower DC power, the common torque command was set to levels between ±0.2pu, as demonstrated by graph (a). The torque demand sequence was selected to change suddenly between these levels to represent possible transient power conditions with the corresponding DC power, and to clearly demonstrate the occurrence of the re-generated propulsion and bow-thruster power due to the mechanical inertia of the rotating propellers. Graph (b) of Fig. 10 illustrates the resulting speeds of the shafts of the propulsion and bow-thruster units whilst graph (c) demonstrates the corresponding DC power for both groups of units, respectively. The total DC-bus power is shown in graph (d). Given this total power, the SC power for the three functions to regulate the DC-bus voltage are shown in the corresponding graph (e). Clearly, when using function 3 (f_3), the SC power fluctuates the least resulting in the lowest DC power exchange, but as shown in graph (f), this function results in the highest fluctuation in the DC-bus voltage. However, since this fluctuation is within the standard limits (±0.1pu), the

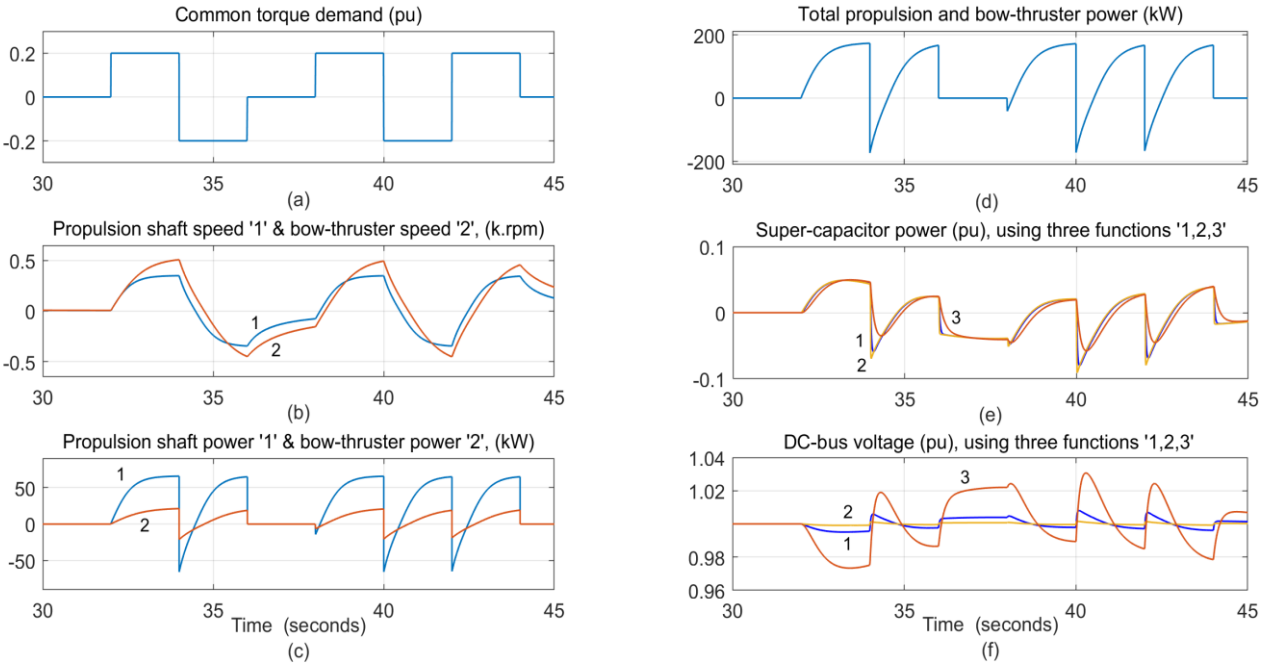

Fig. 10. (a): the pattern of the per-unit torque demand applied simultaneously to all propulsion and bow-thruster units, (b): the corresponding per-unit speeds of the propulsion and bow-thruster units, (c): the corresponding power of both the propulsion units and the bow-thrusters, (d): the total DC power for all propulsion and bow-thruster units, (e): the corresponding super-capacitor power when using the three DC-bus control functions (f_1, f_2, f_3) at k=55 for f_2, f_3, (f): the fluctuation of the DC-bus voltage when using these functions.

performance is acceptable, and the system has the advantage of exploiting the electrical energy stored within the DC-bus components. In comparison, utilizing function 2 (f_2), gave the best performance in terms of regulating the DC-bus voltage but at the expense of generating the highest fluctuation in the SC power, although there is little difference from the SC power generated by function 1. When using functions 1 and 2, the system will not be able to fully exploit the energy stored in the DC-link capacitance or any other energy storage devices added by any modular expansion. A trade-off selection amongst the non-linear functions can be carried out to optimize for specific performance according to the application and the specification of the energy storage components used.

8.2. Performance tests and comparison

The full system operation using the proposed control structure was tested and compared with the low/high-pass filter or frequency-division method, reported in [25] and [26], under severe and transient DC loading conditions that can represent the worst-case scenario of the ship electrical load. For this, a heavy and reversing torque demand pattern, changing between its highest and lowest levels (±1pu), was applied to all propulsion and bow-thruster units, as demonstrated via trace 1 of graph (a) in Fig. 11. Trace 2 of the same graph illustrates the corresponding total DC power, where the negative part of the power represents the re-generative power at instants of changing the direction of the common torque command. This re-generated power, which is transformed from the kinetic energies stored in the rotating parts of the propulsion and bow-thruster units, is absorbed by the SC through the DC-bus. As a reaction to the transient change in the torque or the total power, graph (b) shows the resulting SC power as trace 1 and the

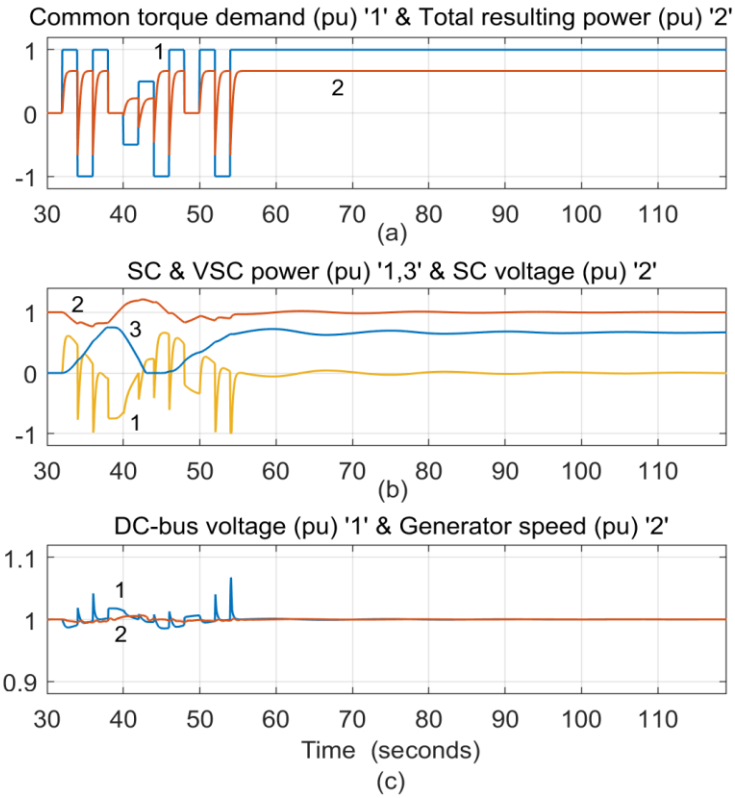

Fig. 11. (a)-(c): Test results when utilizing the proposed V_{sc} closed-loop control method with f_2, (a): the pattern of the per-unit torque demand applied simultaneously to all propulsion and bow-thruster units and the corresponding total DC-power for a worst-case scenario, (b): the corresponding per-unit super-capacitor power '1' and its voltage '2' and the per-unit VSC power '3', (c): the fluctuation in the DC-bus voltage '1' and in the DEG speed '2'.

change in the SC voltage as trace 2, whilst trace 3 demonstrates the variation of the corresponding VSC power when utilizing function 2. It can be realized that the reaction of the SC power controller to any change in the DC-bus voltage resulted in the variation in the DC-bus always being maintained within the permitted limits of ±0.1pu, but mostly around ±0.02pu as illustrated via trace 1 of graph (c). It is clearly shown that the VSC power varies relatively slowly within the given 5s period, which reduces the stress on the DEGs leading to a smooth and negligible fluctuation in the DEGs speed or frequency as demonstrated via trace 2.

Graphs (a) and (b) of Fig. 12 represent the same results but obtained when utilizing the frequency-division or the low/high-pass filter method. This method uses a high-pass filter to pass the high-frequency components of the DC-bus voltage error to an SC power controller in an open-loop manner, whilst leaving the low-frequency components to pass to a battery power controller. For comparison, this method was implemented under the same test conditions used for the proposed control method but with a 0.1Hz cut-off frequency to bring its results to an appropriate level for comparison. The cut-off frequency of the filter used in [25] was comparatively high (1Hz) so could not be used for comparing the performance of the two methods. The characteristics of the low/high-filter method are clearly demonstrated; the resulting variation in the VSC power is not as smooth as that obtained using the proposed control

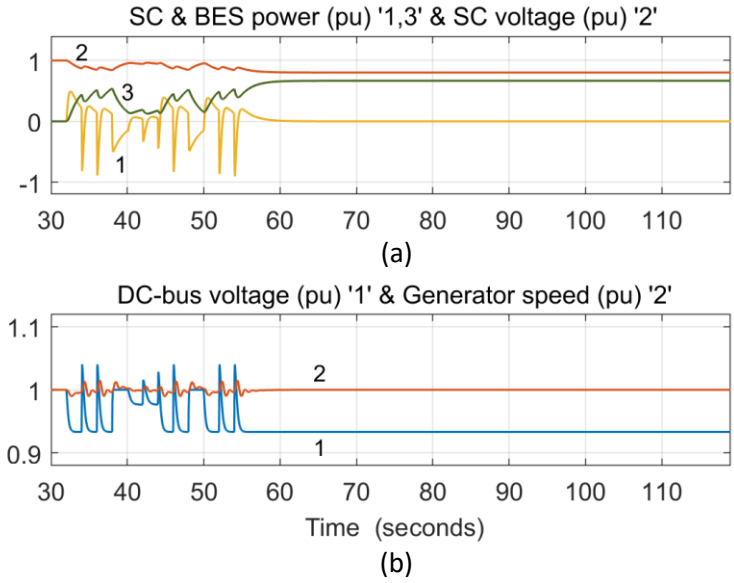

Fig. 12. (a), (b): Test results when utilizing the low/high-pass filter method reported in [25], [26]. All graphs are repeated but using the filter method for comparison.

method, and the SC voltage always varies below its set-point value, as a result of the filter open-loop structure. In other words, the SC voltage has no mechanism to return back to its set-point or its reference value, even when it drifts down as a result of any internal or external leakage currents. It should be noted that trace 3 in graph (a) represents the battery energy storage (BES) power demanded via the low-pass frequency components through the BES DC-DC converter. Graph (b) illustrates that a relatively large offset is associated with the resulting fluctuation in the DC-bus voltage (trace 1), which always keeps the DC voltage below its set-point or nominal value with significant fluctuations, and the DEGs speed (trace 2) is comparatively affected by the unsmooth variation in the BES power demonstrated by trace 3 of graph (a).

In Figs (11) and (12), after 60s run time, it can be realized that for both methods the VSC and BES power are the primary sources for supplying the DC loads or the propulsion and bow-thruster power. However, the SC storage capability is not fully utilized when using the filter method (Fig. 12) as its voltage is always biased due to the lack of a re-balancing mechanism. Also, using this method led to a sustained offset in the DC-bus voltage, even when the DC power was no longer fluctuating. The advantage of utilizing the proposed method for controlling the SC voltage in a closed-loop manner is clearly demonstrated in comparison with the low/high-pass filter or frequency-division method reported in the literature.

To demonstrate the features of using function 3 (f_3) for comparison with the frequency-division method, Fig. 13 shows the results obtained under the same test conditions as for the above scenario. The utilization of this non-linear hyperbolic function permits a wide relaxation in the DC voltage fluctuation within the range from 0.9pu to 1.1pu, allowing a maximum utilization of the DC-bus capacitive energy storage, whilst reflecting a smooth variation on the DEG power through the VSC power. The results also demonstrate a very low fluctuation in the DEG speed/frequency. It should be noted that the slight increase in the DC-bus voltage above its maximum limit at time

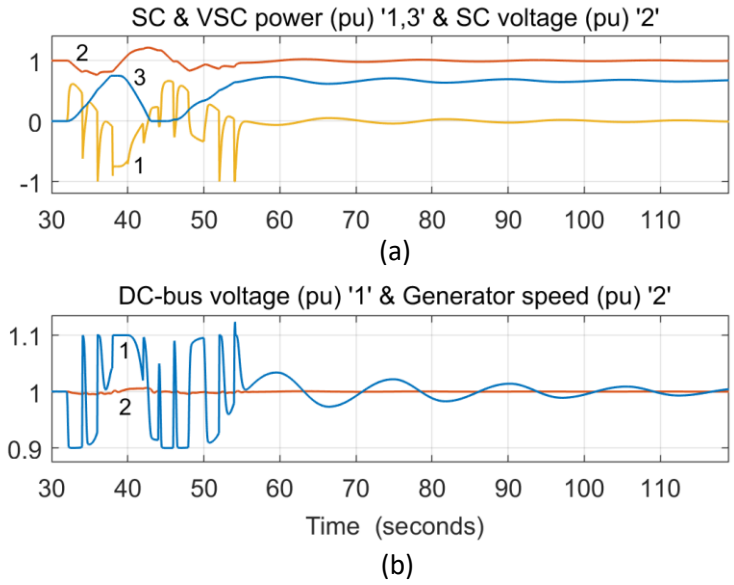

Fig. 13. (a), (b): Test results when utilizing the proposed V_{sc} closed-loop control method with f_3, (a): the corresponding per-unit super-capacitor power '1' and its voltage '2' and the per-unit VSC power '3', (b): the fluctuation in the DC-bus voltage '1' and in the DEG speed '2'.

54s (Fig. 13(b), trace 1) occurred as result of limiting the SC power to -1pu at this time, but this increase can be tolerated. The slight decaying oscillation in the DC voltage around its set-point or nominal value is quite tolerable, as this can be outweighed by considering the necessary mechanism for re-balancing the SC voltage.

9. Conclusion

This paper has presented and discussed an AC/DC microgrid architecture that forms the main part of a vessel power system with electric propulsion and bow-thruster units. To enhance the performance and response of the power system, the paper proposed a new closed-loop control structure which employs a 20F SC as a short-term energy storage unit to support the DC-bus voltage and the speed/frequency of the diesel generators. As both the propulsion and bow-thruster units of the vessel are supplied directly through the DC-bus, they may cause an immediate and severe effect on the generator frequency under uncertain and transient loading conditions. It has been demonstrated through the results presented in the paper that the proposed control structure, using the SC energy storage unit, is very effective under harsh operational scenarios when sudden and reversing torque demands take place for both the propulsion and bow-thruster units. The energy storage unit effectively absorbed the re-generated power due to deceleration of the propellers, and the action of the proposed control method was clearly demonstrated when handling such a reversal of power. Through a suitable design of the control system with an SC voltage re-balancing controller, it was illustrated how this system prevented the speed of the generators from dropping below its standard lower limit. The paper also presented results obtained when using the frequency-division or low/high-pass filter method for controlling the SC power, as reported in the literature, for comparison with the proposed control method. Due to the lack of SC voltage re-balancing, the filter method does not guarantee sustained operation of the SC energy

storage unit and there is a DC voltage offset below the nominal voltage as demonstrated in the final comparison. The effectiveness of the proposed method is clearly demonstrated.

10. Acknowledgements

The work presented in this paper was primarily conducted whilst Faysal Hardan was a Visiting Academic/Research Fellow at Newcastle University. He gratefully acknowledges the sponsorship granted by Newcastle University for his extended fellowship to carry out the main research reported in this paper.

11. References

[1] W. Feng, M. Jin, X. Liu, Y. Bao, C. Marnay, C. Yao, J. Yu, "A review of microgrid development in the United State – A decade of progress on policies, demonstrations, controls, and software tools," Applied Energy, vol. 228, pp. 1656-1668, 2018.

[2] A. Hirsch, Y. Parag, J. Guerrero, "Microgrids: A review of technologies, key drivers, and outstanding issues," Renewable and Sustainable Energy Reviews, vol. 90, pp. 402-411, 2018.

[3] N. Hatziargyriou, H. Asano, R. Iravani, C. Marnay, "Microgrids," IEEE Power and Energy Magazine, vol. 5, no. 4, pp. 78-94, 2007, DOI: 10.1109/MPAE.2007.376583.

[4] S.M. Dawoud, X. Lin, M.I. Okba, "Hybrid renewable microgrid optimization techniques: A review," Renewable and Sustainable Energy Reviews, vol. 82, pp. 2039-2052, 2018.

[5] J. Hu, Y. Shan, Y. Xu, JM. Guerrero, "A coordinated control of hybrid ac/dc microgrids with PV-wind-Battery under variable generation and load conditions," Electrical Power and Energy Systems, vol. 104, pp. 583-592, 2019.

[6] C. Qi, K. Wang, Y. Fu, G. Li, B. Han, R. Huang, T. Pu, "A Decentralized Optimal Operation of AC/DC Hybrid Distribution Grids," IEEE Trans on Smart Grid, vol. 9, no. 6, pp. 6095-6105, 2018.

[7] E. Unamuno, JA. Barrena, "Hybrid ac/dc microgrid-Part I: Review and classification of topologies," Renewable and Sustainable Energy Reviews, vol. 52, pp. 1251-1259, 2015.

[8] Q. Jiang, M. Xue, G. Geng, "Energy Management of Microgrid in Grid-Connected and Stand-Alone Modes," IEEE Trans on Power Systems, vol. 28, no. 3, pp. 3380-3389, 2013.

[9] Y. Chen, S. Zhao, Z. Li, X. Wei, Y. Kang, "Modeling and Control of the Isolated DC–DC Modular Multilevel Converter for Electric Ship Medium Voltage Direct Current Power System," IEEE Journal Emerging and Selected Topics in Power Electronics, vol. 5, no. 1, 2017.

[10] C. Chakraborty, H. Ho-chiang Iu, D. Dah-chuan Lu, "Power Converters, Control, and Energy Management for Distributed Generation," IEEE Trans on Industrial Electronics, vol. 62, no. 7, 2015.

[11] AA. Eajal, MF. Shaaban, K. Ponnambalam, EF. El-Saadany, "Stochastic Centralized Dispatch Scheme for AC/DC Hybrid Smart Distribution Systems," IEEE Trans on Sustainable Energy, vol. 7, no. 3, 2016.

[12] W. Jing, C.H. Lai, S.H.W. Wong, M.L.D. Wong, "Battery-supercapacitor hybrid energy storage system in standalone DC microgrids: a review," IET Renewable Power Generation, vol. 11, no. 4, pp. 461-469, 2017.

[13] FD. Kanellos, GJ. Tsekouras, J. Prousalidis, "Onboard DC grid employing smart grid technology: challenges, state of the art and future prospects," IET Electrical Systems in Transportation, vol. 5, no. 1, pp. 1-11, 2015.

[14] K. Kim, K. Park, G. Roh, K. Chun, "DC-grid system for ships: a study of benefits and technical considerations," Journal of International Maritime Safety, Environment Affairs, and Shipping, vol. 2, no. 1, pp. 1-12, 2018.

[15] Z. Jin, G. Sulligoi, R. Cuzner, L. Meng, JC. Vasquez, JM. Guerrero, "Next-Generation Shipboard DC Power System," IEEE Electrification Magazine, June 2016, pp. 45-57.

[16] B. Zahedi, LE. Norum, KB. Ludvigsen, "Optimized efficiency of all-electric ships by dc hybrid power systems," Journal of Power Sources, vol. 255, pp. 341-354, 2014.

[17] W. Zhu, J. Shi, S. Abdelwahed, "End-to-end system level modeling and simulation for medium-voltage DC electric ship power systems," Naval Architecture and Ocean Engineering, vol. 10, pp. 37-47, 2018.

[18] D. Kumar, F. Zare, "A Comprehensive Review of Marine Microgrids: System Architectures, Energy Efficiency, Power Quality, and Regulations," IEEE Access, vol. 7, pp. 67249-67277, 2019.

[19] S.G. Jayasinghe, L. Meegahapola, N. Fernando, Z. Jin, J.M. Guerrero, "Review of Ship Microgrids: System Architectures, Storage Technologies and Power Quality Aspects," Inventions, 2, 4, 2017, doi: 10.3390/inventions2010004.

[20] M.D.A. Al-Falahi, T. Tarasiuk, S.G. Jayasinghe, Z. Jin, H. Enshaei, J.M. Guerrero, "AC Ship Microgrids: Control and Power Management Optimization," Energies, 11, 1458, 2018, doi: 10.3390/en11061458.

[21] J.J. Valera-Garcia, I. Atutxa-Lekue, "On the Optimal Design of Hybrid-Electric Power Systems for Offshore Vessels," IEEE Trans on Transportation Electrification, vol. 5, no. 1, pp. 324-325, 2019.

[22] S. Faddel, A. A. Saad, M. El Hariri, O. A. Mohammed, "Coordination of Hybrid Energy Storage for Ship Power Systems with Pulsed Loads," IEEE Transaction on Industry Application, vol. 56, no. 2, pp. 1136-1146, 2020.

[23] J. P. Trovão, F. Machado, P. G. Pereirinha, "Hybrid electric excursion ships power supply system based on a multiple energy storage," IET Electrical Systems in Transportation, vol. 6, no. 3, pp. 190–201, 2016.

[24] M.M.S. Khan, M.O. Faruque, A. Newaz, "Fuzzy Logic Based Energy Storage Management System for MVDC Power System of All Electric Ship," IEEE Transaction on Energy Conversion, vol. 32, no. 2, pp. 798-809, 2017.

[25] Z. Xiao, H. Li, H. Fang, Y. Guan, T. Liu, L. Hou, J. M. Guerrero, "Operation Control for Improving Energy Efficiency of Shipboard Microgrid Including Bow Thrusters and Hybrid Energy Storages," IEEE Transactions on Transportation Electrification, vol. 6, no. 2, pp. 856-868, 2020.

[26] Z. Jin, L. Meng, J. M. Guerrero, R. Han, "Hierarchical Control Design for a Shipboard Power System with DC Distribution and Energy Storage Aboard Future More-Electric Ships," IEEE Transaction on Industrial Informatics, vol. 14, no. 2, pp. 703-714, 2018.

[27] Y. Wang, L. Wang, M. Li, Z. Chen, "A review of key issues for control and management in battery and ultra-capacitor hybrid energy storage systems," eTransportation, vol. 4, 100064, 2020.

[28] https://www.skeletontech.com, accessed on 18 Feb. 2021.

[29] Y. Khersonsky, "New IEEE Power Electronics Standards for Ships," IEEE, April 2011, doi: 10.1109/ESTS.2011.5770909.

[30] F. Hardan, J.A.M. Bleijs, R. Jones and P. Bromley, "Bi-directional power control for flywheel energy storage system with vector-controlled induction machine drive," 1998 Seventh International Conference on Power Electronics and Variable Speed Drives (IEE Conf. Publ. No. 456), London, UK, 1998, pp. 477-482, doi: 10.1049/cp:19980573.

[31] A. Hughes, B. Drury, "Electric Motors and Drives: Fundamentals, Types and Applications," Newnes, Elsevier, 5th edition, Aug. 2019.

[32] M.G. Simoes, C.L. Lute, A.N. Alsaleem, D.I. Brandao, J.A. Pomilio, "Bidirectional floating interleaved buck-boost DC-DC converter applied to residential PV power systems," 2015 Clemson University Power Systems Conference (PSC), Clemson, SC, USA, 2015, pp. 1-8, doi: 10.1109/PSC.2015.7101675.

[33] N. Kondrath, "An Overview of Bidirectional DC-DC Converter Topologies and Control Strategies for Interfacing Energy Storage Systems in Microgrids," Journal of Electrical Engineering, vol. 6, pp. 11-17, 2018, doi: 10.17265/2328-2223/2018.01.002.

[34] F. Hardan, R. Norman, W. Leithead, "Model-based control of a VSC-based power generator with synthetic inertia provision in an isolated micro-grid," IET Generation, Transmission & Distribution, vol. 14, no. 22, pp. 5037-5046, 2020, doi: 10.1049/iet-gtd.2020.0304.

[35] Y. Gui, X. Wang, F. Blaabjerg, D. Pan, "Control of Grid-Connected Voltage-Source Converters: The Relationship Between Direct-Power Control and Vector-Current Control," IEEE Industrial Electronics Magazine, vol. 13, no. 2, pp. 31-40, 2019, doi: 10.1109/MIE.2019.2898012.

[36] T. Hornik and Q. Zhong, "A Current-Control Strategy for Voltage-Source Inverters in Microgrids Based on H$^{\infty}$ and Repetitive Control," IEEE Transactions on Power Electronics, vol. 26, no. 3, pp. 943-952, 2011, doi: 10.1109/TPEL.2010.2089471.

[37] N. Panten, N. Hoffmann, F.W. Fuchs, "Finite Control Set Model Predictive Current Control for Grid-Connected Voltage-Source Converters with LCL Filters: A Study Based on Different State Feedbacks," IEEE Transactions on Power Electronics, vol. 31, no. 7, pp. 5189-5200, 2016, doi: 10.1109/TPEL.2015.2478862.

[38] A. Radwan, I. Khouri and X. Jiang, "Modeling and Control of Current-Source Converter-Based AC Microgrids," 2020 IEEE 8th International Conference on Smart Energy Grid Engineering (SEGE), Oshawa, ON, Canada, 2020, pp. 97-101, doi: 10.1109/SEGE49949.2020.9181969.

[39] J. D. Glover, M. S. Sarma, T. J. Overbye, *Power System Analysis and Design*. 5th ed. Stamford, CT: Cengage Learning, 2012, ch. 11, sec. 1, pp. 590-593.

[40] D. Radan, A. J. Sorensen, A. K. Adnanes, T. A. Johansen, "Reducing Power Load Fluctuations on Ships Using Power Redistribution Control," Marine Technology, Vol. 45, No. 3, pp. 162-174, 2008.

[41] J. M. Apsley, A. Gonzalez-Villasenor, M. Barnes, A. C. Smith, S. Williamson, J. D. Schuddebeurs, P. J. Norman, C. D. Booth, G. M. Burt, J. R. McDonald, "Propulsion Drive Models for Full Electric Marine Propulsion Systems," IEEE Transactions on Industry Applications, vol. 45, no. 2, pp. 676-684, 2009.

Appendix A

1. Per Unit (PU) Base Systems :
   - Base/nominal DC-bus voltage V_{dcn}: 1500V
   - Base/nominal super-capacitor voltage: 900V
   - Base/nominal super-capacitor power V_{scn}: 3MW
   - Base/nominal VSC power: 3MW
   - Base/nominal generator power: 2x1.35MW
   - Base/nominal generator speed: 2π x 50/2
2. Maximum/minimum limits:
   - DC-bus voltage limits: Min: 1350V, Max: 1650V
   - Maximum DC-bus load (propulsion load): 2MW or 0.666pu
   - Super-capacitor voltage limits: Min: 540V, Max: 1150V
   - Super-capacitor maximum current: 5.5kA
   - Diesel generator speed limits: Min: 0.96pu, Max: 1.04pu
3. Electrical and mechanical parameters used:
   - Maximum DC-bus load (propulsion load): 2MW or 0.666pu
   - DC-link/bus capacitor value C_{dc}: 360mF
   - DC-link parallel resistance (including capacitor EPR) G_{dc}: 1/1kΩ
   - Inertia constant of the DC-bus H_{dc}: 0.135s
   - Super-capacitor value C_{sc}: 20F
   - Super-capacitor ESR: 5mΩ
   - Super-capacitor EPR: 40kΩ
   - Time-constant for the VSC power controller τ: 3μs
   - Time-constant for the Super-capacitor power controller τ: 3μs
   - Inertia constant of the generators H_g: 0.3085s
   - Total moment of inertia J: 67.5 [kg.m^2]
   - Mechanical damping factor B: 1.3 [N.m/s]
   - Generator power to VSC power per-unit conversion factor K_{vsc}: 3/2.7

- VSC conversion efficiency ρ_{vsc}: 0.98

4. Parameters of the super-capacitor current/power controller (pu):
   - Proportional gain K_p: 0.01
   - Integral gain K_i: 10
5. Parameters of the super-capacitor voltage balancer/controller (pu):
   - Proportional gain K_{pv}: 0.6
   - Integral gain K_{iv}: 1.2
   - Differential gain K_{dv}: 0.01
   - Controller sampling time T_s: 1ms